

Visualization of superluminal pulses inside a white light cavity using plane wave spatio-temporal transfer functions

H. N. Yum,¹ Y. J. Jang,¹ X. Liu,¹ and M. S. Shahriar^{1,2,*}

¹Department of Electrical Engineering and Computer Science, Northwestern University, Evanston, Illinois 60208, USA

²Department of Physics and Astronomy, Northwestern University, Evanston, Illinois 60208, USA
*shahriar@northwestern.edu

Abstract: In a white light cavity (WLC), the group velocity is superluminal over a finite bandwidth. For a WLC-based data buffering system we recently proposed, it is important to visualize the behavior of pulses inside such a cavity. The conventional plane wave transfer functions, valid only over space that is translationally invariant, cannot be used for the space inside WLC or any cavity, which is translationally variant. Here, we develop the plane wave spatio-temporal transfer function (PWSTTF) method to solve this problem, and produce visual representations of a Gaussian input pulse incident on a WLC, for all times and positions.

© 2012 Optical Society of America

OCIS Codes: (190.0190) Nonlinear optics; (190.5530) Pulse propagation and temporal solitons; (120.2230) Fabry-Perot.

References and links

1. J. Yu, S. Yuan, J. Y. Gao, and L. Sun, "Optical pulse propagation in a Fabry-Perot etalon: analytical discussion," *J. Opt. Soc. Am. A* **18**(9), 2153–2160 (2001).
2. J. K. S. Poon, J. Scheuer, S. Mookherjea, G. T. Paloczi, Y. Huang, and A. Yariv, "Matrix analysis of microring coupled-resonator optical waveguides," *Opt. Express* **12**(1), 90–103 (2004).
3. J. E. Heebner, R. W. Boyd, and Q. H. Park, "SCISSOR solitons and other novel propagation effects in microresonator-modified waveguides," *J. Opt. Soc. Am. B* **19**(4), 722–731 (2002).
4. J. E. Heebner and R. W. Boyd, "Slow' and 'fast' light in resonator-coupled waveguides," *J. Mod. Opt.* **49**(14–15), 2629–2636 (2002).
5. J. E. Heebner, R. W. Boyd, and Q. H. Park, "Slow light, induced dispersion, enhanced nonlinearity, and optical solitons in a resonator-array waveguide," *Phys. Rev. E Stat. Nonlin. Soft Matter Phys.* **65**(3), 036619 (2002).
6. G. S. Pati, M. Salit, K. Salit, and M. S. Shahriar, "Demonstration of a tunable-bandwidth white-light interferometer using anomalous dispersion in atomic vapor," *Phys. Rev. Lett.* **99**(13), 133601 (2007).
7. A. Wicht, K. Danzmann, M. Fleischhauer, M. Scully, G. Müller, and R.-H. Rinkleff, "White-light cavities, atomic phase coherence, and gravitational wave detectors," *Opt. Commun.* **134**(1-6), 431–439 (1997).
8. R. H. Rinkleff and A. Wicht, "The concept of white light cavities using atomic phase coherence," *Phys. Scr. T* **118**, 85–88 (2005).
9. R. Fleischhaker and J. Evers, "Four wave mixing enhanced white-light cavity," *Phys. Rev. A* **78**(5), 051802 (2008).
10. H. N. Yum, M. E. Kim, Y. J. Jang, and M. S. Shahriar, "Distortion free pulse delay system using a pair of tunable white light cavities," *Opt. Express* **19**(7), 6705–6713 (2011).
11. H. Yum, X. Liu, Y. J. Jang, M. E. Kim, and S. M. Shahriar, "Pulse delay via tunable white light cavities using fiber optic resonators," *J. Lightwave Technol.* **29**(18), 2698–2705 (2011).
12. L. Levi, "Spatiotemporal transfer function: recent developments," *Appl. Opt.* **22**(24), 4038–4040 (1983).
13. In modeling a FP, it is customary to consider each mirror to have an anti-reflection coating on one face, and a partially reflecting surface on the other. However, in reality, the partial reflectivity is produced by using layers of dielectric materials. Thus, in order to model properly any potential phase shift, in reflection or transmission at such an interface, it is necessary to take into account the presence of such a layer, which can be considered to be a Bragg grating. When this is done, it is no longer necessary to consider the presence of another surface with an anti-reflection coating.
14. H. Kogelnik, "Coupled wavel theory for thick hologram gratings," *Bell Syst. Tech. J.* **48**(9), 2909–2947 (1969).
15. A. Yariv and P. Yeh, *Optical Waves in crystals* (John Wiley & Sons, 1984).

16. To calculate the phase shift due to the Bragg reflection, we solved the coupled equations presented in Ref. 14 for the case of λ (wavelength) = 1550nm, θ (angle of incidence) = 0, ϕ (slant grating angle) = 0 and σ (conductivity) = 0. The modulated dielectric constant is assumed to be of the form $\varepsilon = \varepsilon_0 + \varepsilon_1 \cos\left[\left(2\pi/\Lambda\right)z\right]$ where ε_0 is the average dielectric permittivity, ε_1 is the modulation amplitude and Λ is the grating period. Λ is chosen to fulfill the Bragg matched condition. We have found that the phase shift for the reflected beam is a constant of $-\pi/2$, independent of the value of ε_1 , which determines the amplitude of the reflectivity. We also found that there is no phase shift for the transmitted wave. Finally, we assumed that the thickness of each BG is infinitesimally small, so that $\Delta v_{\text{Bragg}} \gg \Delta v_{\text{FWHM}}$ where Δv_{Bragg} is a bandwidth of the Bragg reflection and Δv_{FWHM} is a full width half maximum of the FP cavity. Thus, for a particular ε_1 , the Bragg reflection coefficient can be expressed as $\exp(-j\pi/2)\sqrt{R}$ with a constant value of R , within the spectral range of Δv_{FWHM} .
17. A. Yariv, *Optical Electronics* (Oxford University Press, 1990).
18. L. J. Wang, A. Kuzmich, and A. Dogariu, "Gain-assisted superluminal light Propagation," *Nature* **406**(6793), 277–279 (2000).
19. R. W. Boyd and D. J. Gauthier, "Slow and fast light," in *Progress in Optics*: **43**, E. Wolf, ed. (Elsevier, 2002), Chap. 6.
20. A. Kuzmich, A. Dogariu, L. J. Wang, P. W. Milonni, and R. Y. Chiao, "Signal velocity, causality, and quantum noise in superluminal light pulse propagation," *Phys. Rev. Lett.* **86**(18), 3925–3929 (2001).

It is well known that optical cavities can be used to control the group velocity of light. Various configurations of the cavities have been proposed to demonstrate slow-light or fast-light. For example, a Fabry-Perot (FP) cavity has been investigated as a system for producing pulse delays [1]. Micro-resonators, such as coupled-resonator optical waveguides (CROWs) [2] and side-coupled integrated spaced sequence of resonators (SCISSOR) [3–5] have also been investigated for producing slow-light and fast-light. More recently, we proposed the use of so-called White Light Cavities (WLCs) [6–9], to realize a trap-door data buffer system where the delay time achievable far exceeds the limit imposed by the delay-bandwidth constraint encountered in a slow-light based data buffer [10,11].

Briefly, such a buffer consists of two WLCs in series, and works as follows. Each WLC is a high finesse cavity containing a medium inside, which has a negative dispersion when a control beam is applied to it, or virtually no dispersion when the control beam is turned off. Initially, the control fields for both WLCs are turned off, so that the medium inside each WLC has essentially no dispersion, and the cavity transmission band is very narrow. A data sequence with a spectrum that is much broader than this band, and is shifted from the cavity resonance frequency by an amount larger than the pulse bandwidth, is thus fully reflected by the first cavity. When the control beam for the first WLC is turned on, its transmission band becomes wide enough to transmit the data sequence fully, without any distortion. After the data stream passes the first WLC, its control beam is turned off again. The data sequence now bounces back and forth between the two inactive cavities, undergoing very small attenuation in each pass. The data stream can be released by activating the control field for either WLC [10,11].

When the transmission band of the WLC becomes very broad, the group velocity in the intra-cavity medium is close to infinity over this bandwidth. In order to understand properly the behavior of the data buffering system under this condition, it is important to visualize the spatial as well as temporal behavior of the pulse everywhere around the WLC: the reflected pulse, the transmitted pulse, and the pulse inside the cavity. In this paper, we use the transfer function method to realize this visualization.

In the analysis of a pulse propagating through a cavity, the conventional approach considers only the temporal transfer function (TTF), which is defined as the ratio of the (complex) amplitude of the output field to that of an input field at a given frequency. In this method, one starts by determining the Fourier transform (FT) of the input pulse. The FT of the output is then given by the product of the transfer function and the FT of the input pulse.

Inverse Fourier transform (IFT) is then used to determine the temporal shape of the output pulse. The space *after* the cavity is invariant under spatial translation, meaning that an observer at any point after the cavity will see the same temporal profile of the transmitted pulse. Thus, it is not necessary to consider the spatial phase of each frequency explicitly.

This is not the case inside the cavity. As a simple example to illustrate this, consider a FP cavity in vacuum, of length L , with the left mirror at $z = z_L$ and the right mirror at $z = z_R$, so that $z_R - z_L = L$. A pulse of temporal duration τ is moving from left to right, so that its spatial extent is $c\tau$, where c is the speed of light in vacuum. Consider now two observers inside the cavity: A positioned at $z = z_L + a$ and B positioned at $z = z_R - a$. We assume further that $a \ll c\tau$, and $c\tau \ll L$. Assuming that each mirror has a high reflectivity, the pulse will undergo multiple bounces inside the cavity. The observer at A will never see interference between the forward and backward propagating pulses, while the observer at B will see such interferences for some durations. Thus, if we compute the temporal transfer function only for the total field inside the cavity, the distinction between the fields seen at these two locations will not be manifest.

This constraint can be overcome by taking the spatial phase into account explicitly in constructing the transfer function, which yields what we choose to call *plane-wave spatio-temporal transfer functions*, PWSTTFs. This is to be distinguished from what is conventionally known as *spatio-temporal transfer function*, STTF, which is used to describe the propagation of a pulsed image, where the spatial part is the FT of the point-spread function, addressing diffraction [12]. The PWSTTFs, which are functions of position as well frequency, are determined by first finding a self-consistent solution, at a given frequency, for a monochromatic plane wave of infinite spatial and temporal extents, and then determining its (complex) amplitudes before, inside, and after a cavity. The field before the cavity has two parts: one propagating to the cavity, in the right direction, denoted as E_{in} (incident field), and one propagating back from the cavity, to the left, denoted as E_r (reflected field). The field inside the cavity also has two parts: one propagating to the right, denoted as E_f (inside field, moving forward), and one propagating to the left, denoted as E_b (inside field, moving backward). Finally, the field transmitted through the cavity is denoted as E_{out} . The PWSTTFs for the reflected field, the inside forward-moving field, the inside backward-moving field and the output field are then given, respectively, by E_r/E_{in} , E_f/E_{in} , E_b/E_{in} , and E_{out}/E_{in} .

To use the PWSTTF approach for determining the propagation of these fields as functions of both space and time, we decompose an input pulse with a given starting position and a temporal shape into a sum of the E_{in} fields, properly phased with respect to one another. The PWSTTFs are then used to find the corresponding E_r , E_f , E_b and E_{out} . Summing the STTFs for each of these four fields then yields the corresponding fields at all times and for all valid ranges of positions. Of course, this approach is generic, and can be applied to any situation, including an empty cavity. We first verify the prediction of this model by analyzing the behavior of a pulse passing through an empty cavity, and comparing the prediction of the output after the cavity with the one produced by the TTF method. We then apply the technique to the WLC. The output after passing through the cavity produced this way again is verified against the prediction of the TTF method. The resulting model allows us to visualize the behavior of the pulse as it propagates superluminally inside the WLC.

The generic system we consider here is illustrated schematically in Fig. 1. A dispersive medium of length L is placed between two mirrors. For concreteness [13], we model each mirror to be a Bragg grating (BG), each with an intensity reflectivity R that is assumed to be constant over the bandwidth of a test pulse. The medium outside the cavity, on each side, is assumed to be non-dispersive, and of infinite extent. The origin of the z -coordinate is set to be

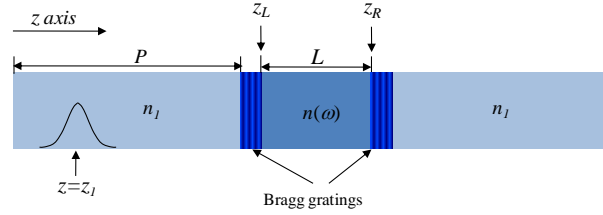


Fig. 1. Schematic illustration of a typical Fabry-Perot (FP) cavity of length L , containing a dispersive medium. We model the mirrors as Bragg gratings. The medium outside the FP is assumed to be non-dispersive. At $t = t_1$, the peak of a test pulse is located at $z = z_1$, moving in the positive z direction

at a distance P from the left BG. The mean indices of the dispersive medium and the non-dispersive medium are n_0 and n_1 , respectively. When $t = t_1$, a Gaussian pulse is centered at $z = z_1$, and moves in the positive z direction. We decompose the pulse into monochromatic waves, calculate phase changes during the propagation through the FP cavity, and use IFT to find the resultant pulse envelope in z domain. To this end, we consider first a monochromatic input wave of unity amplitude, expressed as:

$$E_{in}(\omega, z, t) = \exp(j\phi_{in}); \quad \phi_{in} = k_1(z - z_1) - \omega(t - t_1) \quad (1)$$

where ω is the angular frequency, and $k_1 = n_1\omega/c$, with c being the speed of light in vacuum. In this notation, ϕ_{in} represents the phase at an arbitrary spatio-temporal coordinates $\{z, t\}$, relative to the reference coordinates $\{z_1, t_1\}$.

The wave is reflected by the BG on the left at $z = P$, and then propagates backward. At an arbitrary spatial point z , the reflected wave has accumulated a net spatial phase of $k_1(P - z_1) + k_1(P - z) = k_1(2P - z - z_1)$. In addition, note that, according to the coupled wave theory [14,15], if a wave is reflected by a BG with an arbitrary Bragg-reflection coefficient, then the reflected wave is shifted in phase by $-\pi/2$ [16]. Furthermore, we assume that the BG thickness is infinitesimally small, leading to a Bragg spectral width much larger than that of the FP, so that the reflectivity, \sqrt{R} , can be assumed to be uniform over the bandwidth of interest [16]. The reflected wave therefore can be written as:

$$E_{r1}(\omega, z, t) = \sqrt{R}\exp\left(-\frac{j\pi}{2}\right)\exp(j\phi_{r1}); \quad \phi_{r1} = k_1(2P - z - z_1) - \omega(t - t_1) \quad (2)$$

Note that $\phi_{r1}(z = P) = \phi_{in}(z = P)$.

A part of the wave is also transmitted through the left BG and propagates inside the FP cavity. It is reflected again by the right BG, and returns to the left BG. Therefore, we have to consider two sets of counter-propagating waves. The forward-propagating waves inside the cavity are given by the following infinite series summation:

$$E_f(\omega, z, t) = \sqrt{T}\exp(j\phi_f) \sum_{m=0}^{\infty} \left[R^m \exp(-jm\pi) \exp(2jmk_d L) \right]; \quad (3)$$

$$\phi_f = k_1(P - z_1) + k_d(z - P) - \omega(t - t_1)$$

where T is the transmittance ($R + T = 1$), and k_d is the wave number in the dispersive medium so that $k_d = n(\omega)\omega/c$. Note that ϕ_f contains two spatial phase terms: (i) the term $k_1(P - z_1)$ is due to the non-dispersive medium on the left side of the cavity, and (ii) the term

$k_d(z-P)$ is due to the intra-cavity dispersive medium. Of course, $\phi_f(z=P) = \phi_{in}(z=P)$, as expected. The phases and amplitudes inside the summation account for the multiple bounces, taking into account the phase shift due to reflection from each BG.

Similarly, the backward-propagating waves inside the cavity can be expressed as:

$$E_b(\omega, z, t) = \sqrt{T}\sqrt{R}\exp(j\phi_b) \sum_{m=0}^{\infty} [R^m \exp(-jm\pi) \exp(2jmk_d L)]; \quad (4)$$

$$\phi_b = k_1(P-z_1) + k_d L + k_d(P+L-z) - \pi/2 - \omega(t-t_1)$$

Note that ϕ_b contains three spatial phase terms: (i) the term $k_1(P-z_1)$ is due to the non-dispersive medium on the left side of the cavity, (ii) the term $k_d L$ is due to first leg of the propagation from the left BG to the right BG, through the intra-cavity dispersive medium, and (iii) the term $k_d(P+L-z)$ is due to backward propagation through the intra-cavity dispersive medium after reflection from the right BG. Of course, $\phi_b(z=P+L) = \phi_f(z=P+L) - \pi/2$, as expected, accounting for the extra phase shift due to reflection from the second BG. The phases and amplitudes inside the summation account for the multiple bounces, taking into account the phase shift due to reflection from each BG.

After every bounce inside the cavity, the wave is transmitted through the left BG and then propagates in the $-\hat{z}$ direction. These beams, added together, produce the net additional reflected beam given by:

$$E_{r2}(\omega, z, t) = T\sqrt{R}\exp(j\phi_{r2}) \sum_{m=0}^{\infty} [R^m \exp(-jm\pi) \exp(2jmk_d L)]; \quad (5)$$

$$\phi_{r2} = k_1(P-z_1) + 2k_d L + k_1(P-z) - \pi/2 - \omega(t-t_1)$$

Note that the total reflected field is given by the sum of E_{r1} and E_{r2} . The various terms in ϕ_{r2} can be interpreted in the same manner. As expected, we see that $E_{r2}(z=P) = \sqrt{T}E_b(z=P)$, and $\phi_{r2}(z=P) = \phi_b(z=P)$.

Similarly, using Eq. (3), the overall transmitted field outside the right BG can be expressed as:

$$E_{out}(\omega, z, t) = T\exp(j\phi_{out}) \sum_{m=0}^{\infty} [R^m \exp(-jm\pi) \exp(2jmk_d L)]; \quad (6)$$

$$\phi_{out} = k_1(P-z_1) + k_d L + k_1(z-P-L) - \omega(t-t_1)$$

Note that $E_{out}(z=P+L) = \sqrt{T}E_f(z=P+L)$, and $\phi_{out}(z=P+L) = \phi_f(z=P+L)$, as expected. Finally, we point out that the phase terms resulting from time evolution in Eqs. (1)–(6) have the same sign (minus) to assure that the phase velocity is $+c$ for E_{in} , E_f and E_{out} , and $-c$ for E_{r1} , E_b and E_{r2} .

Summing the infinite series in the expressions above, and using Eq. (2), we find:

$$E_f(\omega, z, t) = \frac{\sqrt{T}}{1 - R\exp(-j\pi)\exp(2jk_d L)} \exp(j\phi_f) \quad (7.a)$$

$$E_b(\omega, z, t) = \frac{\sqrt{R}\sqrt{T}}{1 - R\exp(-j\pi)\exp(2jk_d L)} \exp(j\phi_b) \quad (7.b)$$

$$E_{t_2}(\omega, z, t) = \frac{\sqrt{RT}}{1 - R \exp(-j\pi) \exp(2jk_d L)} \exp(j\phi_{t_2}) \quad (7.c)$$

$$E_r(\omega, z, t) = \sum_{p=1}^2 E_{t_p}(\omega, z, t) \quad (7.d)$$

$$E_{out}(\omega, z, t) = \frac{T}{1 - R \exp(-j\pi) \exp(2jk_d L)} \exp(j\phi_{out}) \quad (7.e)$$

At a first glance, these Eq. (7) may look like the conventional temporal transfer functions (TTF) found in a typical textbook in optoelectronics [17]. However, the key distinction here is the presence of the phase terms, which are functions of not only the temporal coordinate but also of position coordinates. To the best of our knowledge, these expressions have not been presented anywhere else before.

Next, we consider a Gaussian pulse, centered at $z = z_1$ at $t = t_1$, with a spatial half-width (at $1/e$ values) of z_0 . The amplitude of the spatial frequency spectrum of this pulse can be expressed as $\tilde{S}_0(k) = (z_0/\sqrt{2}) \exp[-(k - k_0)^2 z_0^2 / 4]$ where $k_0 = \omega_0/c$, $k = \omega/c$. Each monochromatic component of this pulse acts as an input field of the type expressed in Eq. (1). Applying IFT and using $dk = d\omega/c$, we can now find the pulse everywhere in z -space

$$\text{For } 0 < z < P, S_1(z, t) = 1/\sqrt{2\pi} \int_{-\infty}^{\infty} \tilde{S}_0(k) \left[\sum_{i=in,r} E_i(\omega, z, t) \right] dk \quad (8.a)$$

$$\text{For } P < z < P+L, S_2(z, t) = 1/\sqrt{2\pi} \int_{-\infty}^{\infty} \tilde{S}_0(k) \left[\sum_{i=f,b} E_i(\omega, z, t) \right] dk \quad (8.b)$$

$$\text{For } z > P+L, S_3(z, t) = 1/\sqrt{2\pi} \int_{-\infty}^{\infty} \tilde{S}_0(k) E_{out}(\omega, z, t) dk \quad (8.c)$$

In what follows, we assume, without loss of generality, a situation where $n_0 = n_1 = 1$. First, it is instructive to discuss the pulse propagation in a non-dispersive intra-cavity medium. Figure 2 illustrates the pulse propagating along the z axis, as freeze-frames at different times. For illustration, we consider $R = 0.7$, $T = 0.3$, $P = 500$, $L = 93$, $z_1 = 200$, $z_0 = 10.3746$, free spectral range (FSR) = 1.613MHz, and $\omega_0 = 2\pi \times 1.93 \times 10^{14} \text{ s}^{-1}$ corresponding to the wavelength λ of 1550nm, where all distances are in meters. Thus, the left BG is at $z_L = P = 500$, and the right BG is at $z_R = P + L = 593$. To find the resonance condition for the cavity, it is important to consider the additional phase term due to the Bragg reflections: $\exp(-j\pi)$ in the denominator of Eq. (7.c). Thus, the cavity resonates on the condition that $L = c(2q+1)\pi/(2n_0\omega_0)$ where q is a positive integer. To observe graphically the pulse inside the cavity, q is chosen to fulfill the condition that $L \gg z_0$.

In Fig. 2(a), the incoming pulse is shown at $t = 250/c$. Figure 2(b) illustrates that for $t = 300/c$, the pulse is reflected from the left BG. Note that the interference between E_{in} and E_{r1} is seen over $0 < z < P$. In Fig. 2(c), the incident pulse is split into two pulses after hitting the left BG: the wave given by E_{r1} produces the reflected pulse in $0 < z < P$, and the wave given by E_f produce the forward-propagating pulse inside the cavity. For $t = 390/c$, E_f is

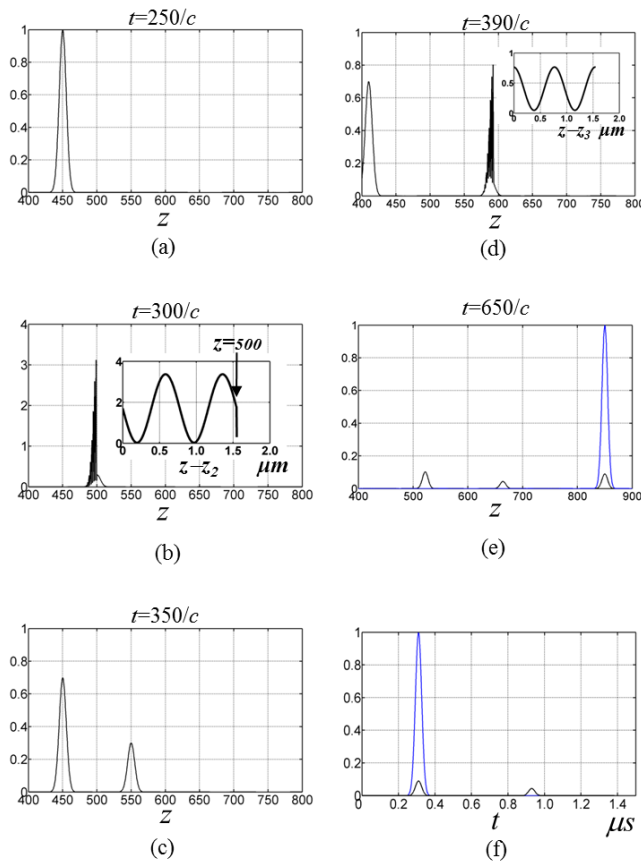


Fig. 2. A propagating pulse shown as freeze-frames for (a) $t = 250/c$, (b) $t = 300/c$, (c) $t = 350/c$, (d) $t = 390/c$, (e) $t = 650/c$. (f) Numerical simulation by the TTF method. The insets present expanded views of the interference patterns. In Fig. 2(e) and 2(f), the reference pulse (blue) propagates together with the first output from the cavity. Note that the left BG is at $z = 500 \equiv z_L$ and the right BG is at $z = 593 \equiv z_R$. For convenience, we have also defined $z_2 = P - \lambda = z_L - \lambda$, and $z_3 = P + L - 3 = z_R - 3$.

reflected by the right BG and then propagates backward, resulting in the backward propagating intra-cavity field E_b . The waves given by E_b and E_f interfere around the front of the right BG, as displayed in Fig. 2(d). These interference patterns are on the scale of the wavelength of light, while the length scales we are considering are macroscopic; as such, the true pattern is masked by the coarseness of sampling. In order to show the pattern clearly, we plot the expanded views over $z_2 < z < z_2 + \lambda$ and $z_3 < z < z_3 + \lambda$ over a distance of one wavelength ($\lambda = 1.55 \mu\text{m}$) in the insets of Fig. 2(b) and 2(d), respectively, where $z_2 = z_L - \lambda$ is a position one wavelength ahead of the left end of the cavity, and $z_3 = 590$ is a position that is 3 meters ahead of the right end of the cavity. These parameters have no particular significance, and have been chosen for illustrative convenience only. Figure 2(e) illustrates that for $t = 650/c$ the backward-propagating pulse (E_b) within the cavity moves toward the left BG. The two pulses in sequence associated with E_{out} propagate with the separation equal to

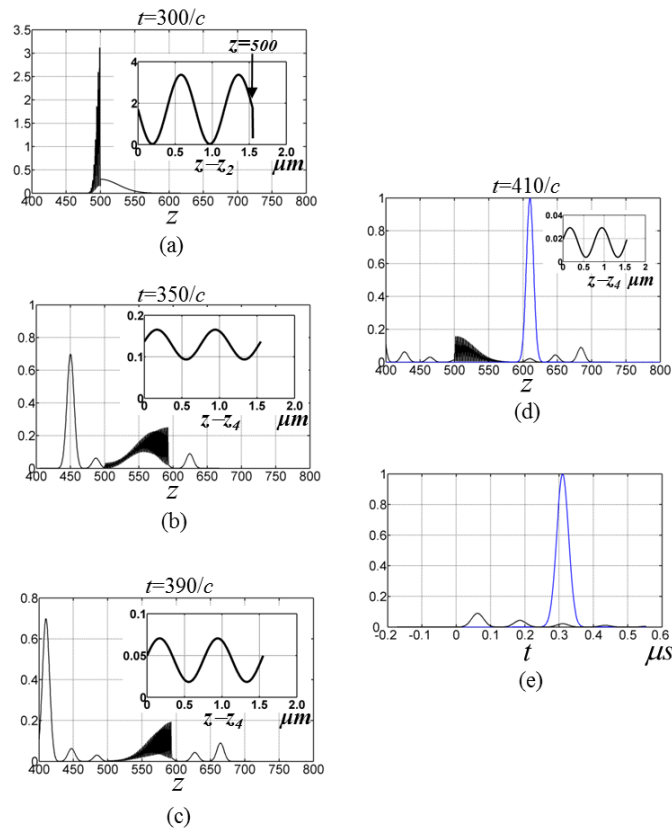


Fig. 3. Propagation of a pulse shown as freeze-frames, for an intracavity fast-light medium with group index $n_g = 0.2$, for (a) $t = 300/c$, (b) $t = 350/c$, (c) $t = 390/c$, (d) $t = 410/c$ with a reference pulse(blue). The insets present expanded views over one wavelength. (e) Output pulses and the reference in time domain.

$2L$, which is the optical path resulting from a round trip inside the cavity. The leading pulse in the output pulse train is observed with no delay compared to the free-space propagating reference (blue) and with the intensity attenuation of 91% due to the cavity reflection.

Note that in this simulation we have used a pulse bandwidth ($\Delta\nu_{pulse}$) that is a factor of 50 larger than the bandwidth of the cavity ($\Delta\nu_{FWHM}$). Since the overlap between the pulse spectrum with the cavity transmission spectrum is negligible, the pulse essentially undergoes sequential reflections at the two BGs, without any significant multi-beam interference. As a result, we do not observe any noticeable distortion, nor delay. In order to verify this result, we have also determined the output pulse using the TTF method [1,10–12], as shown in Fig. 2(f). Here, we see two output pulses in series, with a temporal separation of $2L/c$, in agreement with the distance $2L$ between the two output profiles in the spatial domain, shown in Fig. 2(e).

We consider next the behavior of a pulse propagating through a fast-light intracavity medium, for various sub-unity values of the group index, n_g . To produce anomalous dispersion, we consider dual gain peaks centered around ω_0 , the empty-cavity resonance frequency [6, 18]. The anti-symmetric profile for $n(\omega)$ allows us to set

$n_{02} \equiv (1/2)d^2n/d\omega^2|_{\omega=\omega_0} = 0$. Thus, $n(\omega)$ can be expressed in terms of a Taylor expansion around ω_0 : $n(\omega) = n_0 + (\omega - \omega_0)n_{01} + (\omega - \omega_0)^3 n_{03}$, where $n_{01} = dn/d\omega|_{\omega=\omega_0}$, and $n_{03} = (1/6)d^3n/d\omega^3|_{\omega=\omega_0}$. We employ the same cavity parameters as those used in Fig. 2, and consider only the first order dispersion (n_{01}) in the Taylor expansion of $n(\omega)$.

Figure 3 illustrates the propagation of a pulse for $n_g = 0.2$. At $t = 300/c$, the value of n_g determines the distance between a front edge of the pulse and the right BG. The interference pattern over $z_2 < z < z_2 + \lambda$ are expanded in the inset of Fig. 3(a). The insets of Fig. 3(b)–3(d) illustrate the intracavity interference over $z_4 < z < z_4 + \lambda$, where $z_4 = 550$ represent a position near the center of the cavity. Comparing Fig. 3(a) with Fig. 2(b), both corresponding to $t = 300/c$, we can see the fast-light effect manifestly. In Fig. 2(b), there is no fast-light effect, and the pulse is not stretched. In Fig. 3(a), the group velocity is superluminal, and the front end of the pulse has almost reached the right BG. The intracavity fast-light medium also causes the counter propagating pulses to expand. Thus, the forward-propagating pulse associated with E_f and the backward-propagating pulse associated with E_b interfere with each other over the entire spatial range inside the cavity, as illustrated in Fig. 3(b)–3(d). Figure 3(b) and 3(c) illustrate that the pulse train is composed of the reflected pulse associated with E_{r1} (the first pulse on the left of the cavity), a series of pulses resulting from E_{r2} (remaining pulses on the left of the cavity) and E_{out} on the right of the cavity. Of course, the separation in z -axis between the adjacent pulses corresponds to the optical path for one round trip inside the cavity i.e. $2n_g L$. Figure 3(d) shows that on the right side of the cavity ($z > 593$) the first and the second pulses are advanced by $(n_0 - n_g)L$ and $(n_0 - 3n_g)L$, respectively, compared to the free-space propagating reference, and the third pulse coincides with the reference, since $(n_0 - 5n_g)L = 0$. Note that $(2m+1)n_g L$ is the optical path in the intracavity medium where m is the number of round trips after the pulse hits the right BG for the first time. In Fig. 3(e), the TTF method is used to produce the output pulse train in time domain. The pulses appear with a repetition rate of $2n_g L/c$, in agreement with the spatial profiles shown in Fig. 3(d). By comparison with the reference, we find that the time advancement also agrees with the results displayed in Fig. 3(d). For example, the delay time between the first pulse and the reference is $(n_0 - n_g)L/c$.

Figure 4 illustrates the cases of $n_g \approx 0$ corresponding to the ideal WLC condition. In Figs. 4(a)–4(c), the portion of the pulse that is loaded into the intracavity fast-light medium passes instantly through the cavity. Subsequently, it shows up to the right side after the cavity ($z > 593$) before the rest of the pulse enters into the cavity. Of course, such a fast movement inside the cavity is the obvious manifestation of $v_g \approx \infty$ [19].

In order to understand the behavior of the pulse in this case, it is instructive first to consider the limit where the cavity mirrors are eliminated. In the simulation, this can be achieved simply by setting $T = 1$, $R = 0$ for each BG, corresponding to a free-space zone of infinite group velocity (ZIGV) from $z = 500$ ($\equiv z_L$) to $z = 593$ ($\equiv z_R$). The resulting profiles are shown in the upper insets of each Figs. 4(a)–4(c). As can be seen, when the pulse enters the ZIGV, it gets split immediately, with the front part of the pulse appearing outside this zone on the right. The amplitude of the field in the ZIGV becomes a constant, equaling the value of the pulse amplitude at the point of splitting. More explicitly, we denote by $f(z)$ the shape of

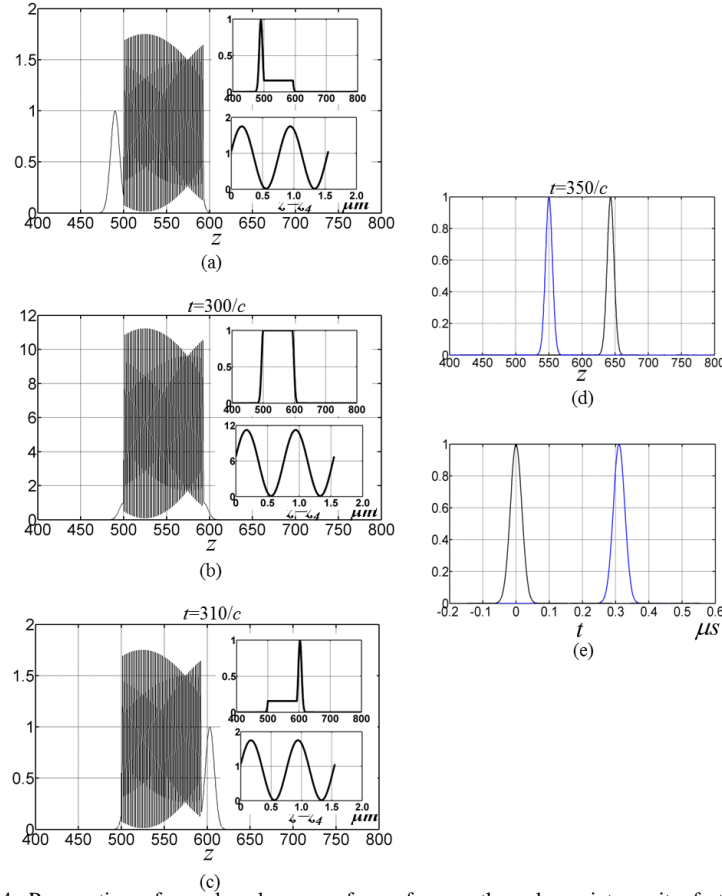


Fig. 4. Propagation of a pulse shown as freeze-frames, through an intracavity fast-light medium under ideal WLC condition ($n_g = 0$) for (a) $t = 290/c$, (b) $t = 300/c$, (c) $t = 310/c$, (d) $t = 350/c$. The upper insets illustrate the case of a fast-light medium with $n_g = 0$ in free space. The lower insets show the views expanded horizontally close to $z_d = 550$. (e) Numerical simulations for cavity output (black) and the reference (blue) in time domain, produced via the TTF method.

the pulse, for $n_g = n_0$, at a time when it has crossed the point $z = z_L$. Then, for $n_g = 0$, we have:

$$\begin{aligned}
 z_L \geq z : E(z) &= f(z); & z_L < z < z_R : E(z) &= f(z_L); \\
 z_R \leq z : E(z) &= f(z - (z_R - z_L))
 \end{aligned}
 \tag{9}$$

The physical meaning of the flat profile inside the ZIGV can be understood by considering the fact that $d\phi/d\omega \equiv (\ell/c)d(n(\omega)\omega)/d\omega = n_g \ell/c$, where ϕ is the phase shift due to the propagation through the medium. For $n_g = 0$, we thus have $d\phi/d\omega = 0$, so that ϕ is constant. The value of the pulse envelope, for example ~ 0.2 at $z = z_L$ as shown in the upper inset of Fig. 4(a), is determined by summing the constituent waves. If the phase differences among the waves before the ZIGV are preserved, the pulse envelope value then

does not change during the propagation through the ZIGV. As a result, the envelope value exhibits the height equal to that at $z = z_L$, for the whole ZIGV, as illustrated in the inset of Fig. 4(a), is determined by summing the constituent waves. If the phase differences among the waves before the ZIGV are preserved, the pulse envelope value then does not change during the propagation through the ZIGV. As a result, the envelope value exhibits the height equal to that at $z = z_L$, for the whole ZIGV, as illustrated in the inset of Fig. 4(a).

This result can also be seen formally from Eq. (7.a), by setting $R = 0$, $T = 1$. We then get $E_f = \exp(j\phi_f)$, where ϕ_f is the phase shift for each wave as it traverses the dispersive zone. For $n_g = 0$, this phase shift is the same for each constituent wave, independent of frequency, as noted above. For the case of the cavity (i.e., $R \neq 0, R+T=1$), the resonance condition [$2k_d L = (2m+1)\pi$] is satisfied for each constituent wave, independent of frequency, for the ideal WLC condition of $n_g = 0$. This can be seen by noting that $k_d = n(\omega)\omega/c$ that, so that $\partial k_d / \partial \omega = (1/c)\partial [n(\omega)\omega] / \partial \omega = (1/c)n_g = 0$, which is akin to the fact that when the group velocity becomes infinite, the wavelength (and therefore the wave number) becomes independent of frequency. As a result, we find from Eq. (7.a) that $E_f = 1/\sqrt{T} \exp(j\phi_f)$, with the value of ϕ_f being the same for each constituent wave. Thus, the pulse amplitude for the forward propagating pulse inside the cavity is also a constant, but larger by a factor of $1/\sqrt{T}$ when compared to the case of free space propagation through the ZIGV. This enhancement is the same as what would be seen for a continuous wave passing through such a cavity on resonance, which results from constructive interference between the infinite number of bounces it undergoes. Here, the forward wave is moving at an effectively infinite velocity, thus carrying out the infinite number of bounces immediately, and yielding the amplitude that would result from the constructive interference of these bounces, since each frequency component is resonant.

Consider next the backward-propagating wave, E_b , as expressed in Eq. (7.b) for each constituent wave. Again, for $n_g = 0$, each wave is resonant, independent of frequency, and the propagation phase, ϕ_b , is the same for each wave, independent of frequency. Thus, within the ZIGV (i.e., within the cavity in this case), the reflected wave is also a constant. For each bounce, the backward-propagating wave is smaller than the corresponding forward propagating wave by a factor of \sqrt{R} , due to the reflection from the right BG, and has relative, constant phase factor of $\exp(-j\pi/2)$ due to this reflection. However, just as in the case of the forward propagating waves, the backward propagating waves also undergo constructive interference between the infinite number of reflections immediately, forming a net wave which is smaller than the net forward wave, E_f , by a factor of \sqrt{R} , and differed by a constant phase factor of $\exp(-j\pi/2)$. Thus, the net field inside the cavity is the result of the interference between these two waves of constant amplitudes, producing a standing wave and a traveling wave (since the amplitudes are different). Of course, the amplitudes of these standing and traveling wave components change with time as the input pulse keeps moving past the entrance at $z = z_L$, as can be seen in Figs. 4(a)–4(c). The intracavity net field can thus be expressed in general as: $f(z_L) \left[1/\sqrt{T} \exp(j\phi_f) + \sqrt{R}/\sqrt{T} \exp(j\phi_b) \right]$. We plot in the lower insets the expanded views over $z_4 < z < z_4 + \lambda$ where again $z_4 = 550$ is a point near the center of the cavity. Note that the maximum ($\equiv E_{\max}$) of the oscillating field amplitude

corresponds to $f(z_L) \left[\frac{1}{\sqrt{T}} + \sqrt{R}/\sqrt{T} \right]$ and the minimum ($\equiv E_{\min}$) to $f(z_L) \left[\frac{1}{\sqrt{T}} - \sqrt{R}/\sqrt{T} \right]$. In particular, the lower inset in Fig. 4(b) indicates that for $f(z_L) \approx 1$, $|S_2(z,t)|^2$ oscillates between $|E_{\min}|^2 = 0.089$ and $|E_{\max}|^2 = 11.24$.

Another important aspect of the result shown in Fig. 4 is the absence of any reflection by the cavity. Of course, this follows from the fact that each constituent wave is resonant for the ideal WLC condition of $n_g = 0$, as discussed above. We can also see this explicitly by considering the expressions for E_{r1} given by Eq. (2) and E_{r2} given by Eq. (7.a), keeping in mind that the net reflected beam is given by the sum of these two. By setting $2k_d L = (2m+1)\pi$ on resonance in Eq. (7.c), we get $E_{r2} = \exp(-j\pi/2)\sqrt{R}\exp(j\phi_{r2})$ where $\phi_{r2} = k_1(P-z_1) + k_1(P-z) - \omega(t-t_1) + \pi$. Comparing this to Eq. (2), we see that $E_{r2} = -E_{r1}$, so that the net reflected field is zero. Since this conclusion is true for each constituent wave, there is no reflection by the ideal WLC.

Finally, Fig. 4(d) illustrates that the pulse emerging from the ideal WLC (black trace) is advanced compared to a reference pulse (blue trace) propagating through a non-dispersive medium of index n_0 . The distance of advancement $(n_0 - n_g)L = n_0 L$, as expected, meaning that the pulse suffers no time delay at all in crossing the WLC. In Fig. 4(e), we show the corresponding result in time domain, again calculated by using the TTF method. The advance in time compared to the reference pulse is in agreement with the result of Fig. 4(d). Of course, we would see the same amount of advancement, in time or space, if we did not use a cavity, but still used a dispersive medium with $n_g = 0$.

We note that this type of advancement using a free space medium cannot be used to violate causality for any real system [18, 20]; the same conclusion holds for an ideal WLC. The apparently unphysical nature of this advancement is attributed to the unavoidable limitation of our model, since the Gaussian input pulse has an infinite temporal extent. If it were possible to model the propagation of a pulse with a true front, we expect to find that the front of the pulse would never propagate faster than the vacuum speed of light. However, such a pulse has an infinite bandwidth, and cannot be studied using the spectral decomposition method employed here. This interpretation is essentially the same as what is offered in explaining the superluminal propagation of a Gaussian pulse envelope through a free-space fast-light medium.

To summarize, in order to understand the behavior of a pulse inside a cavity, we have developed an approach that starts by finding a self-consistent solution for a monochromatic field of infinite spatial and temporal extents, and determine its amplitudes before, inside, and after the cavity. We then construct a Gaussian input pulse by adding a set of these waves, properly phased and weighted, to represent a moving pulse before the cavity. Adding these waves at various time intervals then yields the complete spatial profile everywhere, including before, inside and after the cavity. In particular, it reveals waves in both forward and backward directions, including multiple bounces occurring inside the cavity. This approach is generic, and can be applied to any situation, including an empty cavity. We first confirm the prediction of this model by analyzing the behavior of a pulse passing through an empty cavity, and comparing the prediction of the output with the one produced by the TTF method. We then apply the technique to a cavity containing a fast-light medium. The output pulse produced this way again agrees with the prediction of the TTF method. The resulting model allows us to visualize the behavior of the pulse as it propagates superluminally inside the cavity, and interferes with itself through multiple bounces. For the limiting case of a vanishing group index over the entire bandwidth of the pulse, an interference pattern is formed immediately after the pulse enters the cavity, with an output pulse emerging with no

time delay or distortion. The results obtained here illustrates the physical mechanism behind pulse propagation through a white light cavity, a process we have proposed earlier for realizing a high bandwidth, long delay data buffering system

Acknowledgments

This work was supported by DARPA through the slow light program under grant FA9550-07-C-0030, and by AFOSR under grants FA9550-06-1-0466 and FA9550-10-1-0228, and by the NSF IGERT program under grant DGE-0801685.